Article | Received 6 August 2026; Revised 15 October 2026; Accepted 21 October 2026; Published XX October 2026
https://doi.org/10.55092/bm20260010

# Architecture-controlled carbon nanotube/bottlebrush elastomer–silver nanowire-based multilayer composites for skin-interfaced applications

**Abby Jackson and Yuncheng Du***

Department of Biomedical Engineering, University of Houston, Houston, USA

* Correspondence author; E-mail: ydu20@uh.edu.

## Highlights:

- Engineer conductive composites with tunable structures for electromechanical sensing.
- Sandwich structures with varying AgNW interlayer configurations optimize conductivity.
- Balanced conductivity-sensitivity-compliance achieved by interfacial design.

**Abstract:** Flexible conductive elastomers are promising biofunctional materials for skin-interfaced electronics, soft robotics, and mechanically compliant biomedical devices. However, approaches for tuning electrical transport and deformation-dependent response in conductive soft elastomer composites remain underdeveloped. We report architecture-controlled carbon nanotube/bottlebrush elastomer–silver nanowire (CNT/BBE–AgNW)-based multilayer composites with tunable thickness and interlayer configurations. CNT/BBE layers provide a soft conductive elastomer matrix, while AgNW interlayers introduce engineered conductive interfaces within the multilayer structure. Regular, thin, and double-sandwich architectures were fabricated to evaluate how through-plane transport distance and AgNW interface regulates electrical conductivity, mechanical coupling, and electromechanical behavior. Our results suggest that reducing thickness improved conformability, while using a double-sandwich AgNW architecture enhanced baseline conductivity and transport stability. Wearable bending demonstrations also showed that the regular architecture responded more favorably to localized finger bending, whereas the thin structure responded more strongly to distributed wrist bending because of enhanced conformal coupling. Frequency-dependent cyclic loading further showed that the composites can distinguish low-to-moderate-frequency mechanical inputs. These findings establish thickness and multilayer architecture engineering as promising design strategies to tune CNT/BBE-AgNW-based electromechanical materials for future skin-interfaced and soft biofunctional systems.

**Keywords:** conductive composite materials; interfacial engineering; sandwich architectures; through-plane conductivity; electromechanical stability; wearable sensors; carbon nanotubes; silver nanowires; bottlebrush elastomers

Copyright©2026 by the authors. Published by ELSP. This work is licensed under Creative Commons Attribution 4.0 International License, which permits unrestricted use, distribution, and reproduction in any medium provided the original work is properly cited.

## 1. Introduction

Flexible conductive elastomers are emerging biofunctional materials for skin-interfaced electronics, soft robotics, and mechanically compliant biomedical systems [1]. These materials are expected to combine electrical conductivity with mechanical flexibility, deformability, and conformal contact with biological or irregular soft surfaces. Unlike rigid or conventional materials [2,3], ultra-soft conductive elastomers maintain functional charge transport while undergoing bending, stretching, compression, and repeated contact deformation [4,5]. Achieving this combination remains challenging since conductive networks embedded in elastomer matrices rearrange under deformation, therefore leading to changes in resistance, signal drift, hysteresis, or unstable electrical response during repeated use [6–8].

A common strategy for making soft electromechanical materials is to incorporate conductive fillers into elastomeric matrices. For example, carbon nanotubes (CNTs), graphene derivatives, carbon black, and silver nanowires (AgNWs) have been used to form percolated conductive networks within soft polymers [7,9,10]. In these systems, electrical transport is governed by filler dispersion, conductive junction density, and tunneling distance [11,12]. Mechanical deformation changes the geometry and connectivity of the conductive network, which produces measurable resistance changes. This deformation-dependent resistance modulation is useful for wearable motion monitoring, human–machine interfaces, and soft robotic proprioception, but it also introduces challenges because conductive junctions can be disrupted, reformed, or displaced during repeated loading [13,14]. Therefore, material architectures that improve conductive-pathway continuity while preserving mechanical compliance are important for developing reliable soft electromechanical materials.

Among various conductive fillers, AgNW networks have emerged as particularly attractive architectural approaches as they can form highly interconnected conductive pathways while maintaining flexibility. For example, AgNW-based flexible sensors demonstrated that nanowire density, junction quality, and percolation structure strongly affect sensitivity and electrical stability [15]. Engineered nanostructured interfaces, such as interlocking nanofiber structures, have also demonstrated that contact geometry and interfacial design can substantially affect electromechanical response [16]. Moreover, AgNW/polymer composite films have been investigated as stretchable electrodes and soft conductive layers, illustrating the broader role of AgNW networks as functional interfaces beyond conventional strain sensing [17].

While conductive networks affect charge transport, the elastomer matrix largely governs the mechanical compliance, stretchability, and conformability of base composite. Consequently, optimizing conductive fillers alone is insufficient and careful selection of elastomer matrix is equally important for the design of biofunctional materials. Recent studies have demonstrated that bottlebrush elastomers (BBEs) provide a promising matrix for ultra-soft biofunctional materials because of their low modulus, high compliance, and tissue-like mechanical behavior [18]. For example, polydimethylsiloxane (PDMS) based BBEs have been reported with Young's modulus values below 1 kPa [18], including a pure PDMS BBE modulus of approximately 0.63 kPa, while conductive CNT/BBE composites with 0.4–0.6 wt.% CNT remained in the ultra-soft range with reported Young's modulus values below 11 kPa [19]. These reported values support the use of BBE as an ultra-soft matrix platform, although direct mechanical characterizations of the CNT/BBE–AgNW multilayers remain needed.

Their molecular structure allows the formation of elastomeric networks that deform readily under small external forces, thus making them attractive for skin-interfaced and soft biomedical devices [19, 20]. However, while BBEs provide clear mechanical advantages, they can only act as electrical insulators without added conductive fillers such as CNTs [21]. Although various approaches have been developed to improve electrical properties of BBEs by incorporating conductive materials, controlling electrical transport in BBE-based conductive composites remains challenging [18,22]. In particular, through-plane charge transport across multilayer BBE-based systems has not yet been systematically studied. In this case, the effects of structural thickness, conductive interlayer placement, and multilayer architecture on electrical and electromechanical behavior of BBE-based composites remain insufficiently understood [19,20,22].

Additionally, although AgNW networks and BBEs have each demonstrated its significant advantages, integrating them into architecture-controlled conductive composites remains relatively unexplored. Prior studies on CNT/elastomer composites have shown tunable piezoresistive behavior through adjustments in filler concentration, network morphology, and elastomer composition [7,8]. AgNW-based elastomers have also shown stretchability, conductivity, and deformation-responsive resistance changes through percolating nanowire networks [9,10]. More complex sandwich structures combining CNTs, AgNWs, or other conductive networks have been reported in conventional elastomer matrices such as PDMS and related polymers [23]. However, these studies generally focus on device-level sensing performance or filler-network optimization, while the influences of multilayer architecture in regulating through-plane transport, conductive-interface density, and deformation-dependent resistance modulation in a soft BBE matrix remains insufficiently understood [24]. Considering that, the goal of this work is not to study the combination of individual uses of CNTs or AgNWs, nor from introducing a new sensing mechanism. Instead, the focus in this work lies in using multilayer architecture and AgNW interfacial placement as design variables to tune the conductivity–response balance in CNT/BBE-based soft electromechanical materials.

The contribution in this current work thereby lies not in the individual use of CNTs or AgNWs to fabricate conductive materials, but in the architecture-controlled integration of soft CNT/BBE conductive matrix with AgNW interfacial network density. Specifically, this study fabricates and compares regular, thin, and double-sandwich CNT/BBE–AgNW multilayer composites to evaluate two architectural variables: composite thickness and interlayer configuration. These architectures allow comparison of how through-plane transport distance and conductive-interface number affect the baseline resistance and deformation-dependent resistance response. To establish a foundation for future device-level optimization of skin-interfaced biomedical sensors and soft electromechanical devices, this work focuses on materials design and architecture–property relationships rather than complete sensor validation.

Using the fabricated materials, wearable finger- and wrist-bending tests are included as demonstrations of skin-interfaced material functionality rather than as complete sensor validation. These demonstrations provide examples of how architecture affects deformation-dependent resistance response under localized and distributed body motion. Frequency-dependent cyclic loading is also used to evaluate whether the composites can distinguish controlled mechanical inputs under low-to-moderate-frequency excitation. These studies together establish thickness and AgNW interface density as design parameters for tuning the conductivity–sensitivity balance in CNT/BBE-AgNW-based ultra-soft electromechanical materials. This architecture-guided materials design may support future skin-interfaced electronics, soft wearable interfaces, and flexible robotic proprioceptive systems.

## 2. Materials and methods

### *2.1. Materials*

In this work, polydimethylsiloxane (PDMS; MCR-M11, Gelest) and crosslinker (DMS-R22, Gelest) were used to synthesize BBEs with azobisisobutyronitrile (AIBN, Sigma-Aldrich) as a thermal initiator. Additionally, single-walled CNTs (0.6 wt.%) were dispersed into precursors in order to make CNT/BBE composites, which were then cast, degassed, and thermally cured at 80 °C in a vacuum oven [22]. AgNW dispersed in isopropyl alcohol were used to prepare conductive interlayers between CNT/BBE layers for investigating how multilayer design affects electromechanical response.

### *2.2. Preparation of CNT/BBE composite layers*

CNT/BBE composites were prepared through mixing PDMS and crosslinker at a molar ratio of 600:1 with 2 mol.% AIBN based on previous literature optimization [20,22]. CNTs were added at 0.6 wt.% relative to the precursor mixture. In order to obtain a homogeneous dispersion while limiting premature curing or crosslinking, the resulting mixture was stirred magnetically for 90 min in an ice bath. The CNT/BBE precursor was further cast into PTFE molds, degassed under vacuum overnight, and thermally cured at a temperature of 80 °C for 12 h to form elastomer layers.

Layer thickness was controlled during casting by adjusting the precursor volume. Thickness values were measured by using a digital caliper. Since the AgNW interlayers were nanoscale coatings relative to the millimeter-scale CNT/BBE layers, the total device thickness was primarily estimated by the CNT/BBE layer dimensions.

### *2.3. AgNW interlayer deposition*

AgNW interlayers were deposited onto the cured CNT/BBE surfaces by spray coating. Before AgNW deposition, CNT/BBE substrates were treated with oxygen plasma to improve surface adhesion. AgNW suspensions with a concentration of 0.2 wt.% in isopropyl alcohol were sprayed using an airbrush at approximately 29 psi, a spray distance of approximately 12 cm, and a nozzle size of 0.8 mm [25]. Eight spray cycles were applied, with approximately 30 s between cycles to allow rapid solvent evaporation. After deposition, samples were annealed at 60 °C for about 10 min.

### *2.4. Fabrication of multilayer composites*

CNT/BBE–AgNW sandwich composites were fabricated by stacking CNT/BBE layers and AgNW-coated interfaces. A small amount of uncured CNT/BBE precursor was also applied between layers as an adhesive interfacial bonding layer, which was followed by post-curing at a temperature of 80 °C for 1 h to promote bonding between stacked components.

Specifically, Figure 1 illustrates the design and fabrication of CNT/BBE–AgNW sandwich composites with controlled thickness and interfacial architecture. Three configurations were prepared: a regular sandwich structure, a reduced-thickness thin structure, and a double-sandwich structure incorporating an additional AgNW interlayer (Figure 1a). These architectures were selected to

independently examine the effects of through-plane transport distance and conductive interface density on the electromechanical behavior of the fabricated CNT/BBE–AgNW composites.

The overall fabrication process is also summarized in Figure 1b. In brief, CNTs were first dispersed into BBE precursors and cured to form conductive elastomer layers. AgNW networks were then deposited onto plasma-treated CNT/BBE surfaces by spray coating. The AgNW-coated CNT/BBE layers were subsequently stacked with additional CNT/BBE layers using a thin layer of uncured CNT/BBE precursor as an interfacial adhesive, followed by post-curing to promote bonding. The regular and thin structures contained one AgNW interlayer, while the double-sandwich structure contained two AgNW interlayers. The thin structure reduced the through-plane transport distance, whereas the double-sandwich structure increased conductive interface density while maintaining a total thickness comparable to the regular architecture. Electrical continuity was visually examined by LED illumination (Figure 1c), which helped confirm that conductive pathways were successfully formed across the multilayer structure.

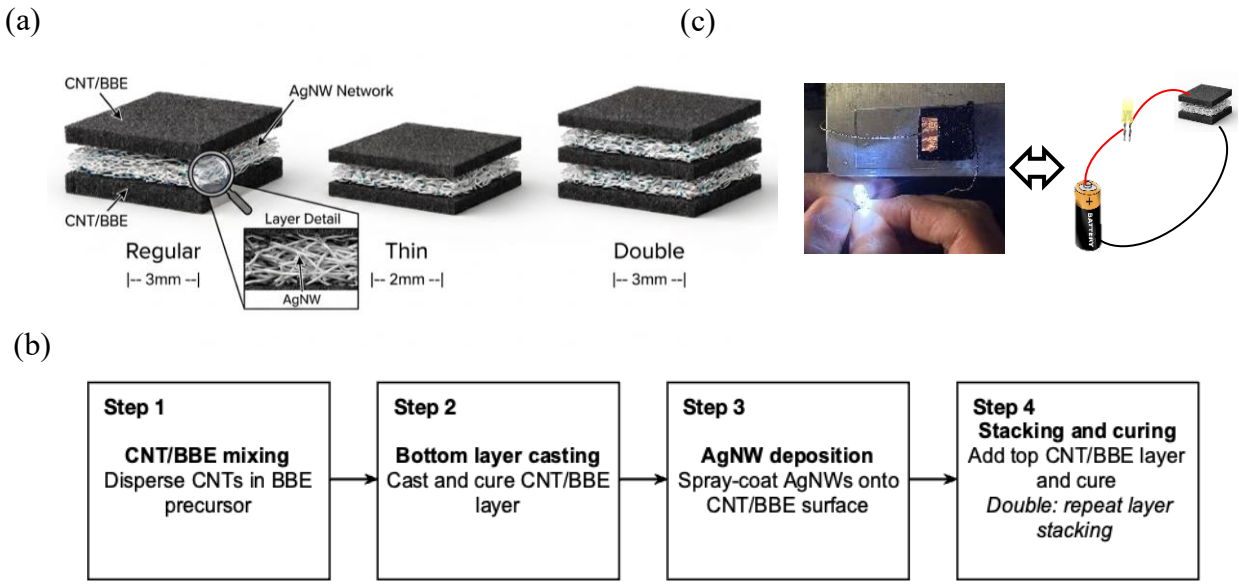



**Figure 1.** Architecture and fabrication of the CNT/BBE–AgNW sandwich composites. **(a)** Schematic of regular, thin, and double sandwich configurations; **(b)** Overview of the fabrication process; **(c)** Optical demonstration and confirmation of electrical conductivity.

### *2.5. Morphological and compositional characterization*

The morphology and composition of the AgNW interlayer were first characterized before encapsulation. Scanning electron microscopy (SEM) was used to study surface morphology of CNT/BBE after AgNW deposition. Higher-magnification SEM imaging was collected and used to evaluate the formation of interconnected AgNW networks. Energy-dispersive X-ray spectroscopy mapping was used to identify elemental distributions of C, O, Si, and Ag within the interlayer region. Quantitative EDS analysis was used to confirm the presence of Ag from the nanowire network. Cross-sectional SEM was also performed after electromechanical testing to determine whether the multilayer structures remained mechanically integrated. Additionally, atomic force microscopy (AFM) was employed to quantitatively characterize and visualize the three-dimensional deposition of AgNW interlayer.

*2.6. Electrical characterization*

Baseline electrical properties were measured using a Keithley 2614B sourcemeter under a through-plane electrode configuration, which is schematically shown in Figure 2. The top and bottom electrodes in this configuration were placed on opposite surfaces of the hybrid materials, forcing current to pass through the multilayer architecture. In this way, this geometry was expected to enable the evaluation of vertical charge transport across the top and bottom CNT/BBE encapsulation layers and the AgNW interlayers.

For characterization, a constant current of 100 μA was applied and the resulting voltage was recorded to estimate resistance. Electrical conductivity was estimated based on the baseline resistance and sample geometry using:

$$\boldsymbol{\sigma = \frac{L}{R \cdot A}} \quad (1)$$

where $\sigma$ represents the conductivity, $L$ defines the thickness of composites, $A$ is the electrode contact area, and $R$ denotes the measured resistance. The electrode contact area was 6.35 mm × 25 mm. Because the through-plane configuration may produce a non-uniform current path in the composites, the calculated resistivity and conductivity values therefore should be interpreted as apparent, geometry- and electrode-configuration-dependent comparative metrics rather than intrinsic material constants.

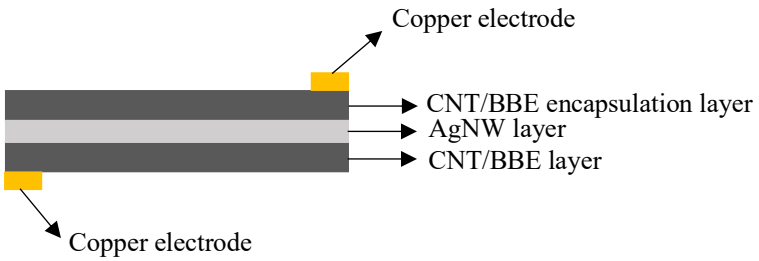



**Figure 2.** Schematic of the through-plane electrode configuration for electrical and electromechanical measurements, illustrating the CNT/BBE layers, AgNW interlayer, and copper electrode placements.

*2.7. Electromechanical characterization*

To illustrate the potential applications of the multilayer CNT/BBE–AgNW materials, electromechanical sensing was performed and used for evaluation under finger and wrist bending. For wearable bending tests, CNT/BBE–AgNW composites were attached to the target joint region, and resistance was recorded in real time during repeated deformation and relaxation cycles. The normalized resistance change was estimated as:

$$\boldsymbol{\frac{\Delta R}{R_0} = \frac{R - R_0}{R_0}} \quad (2)$$

where $R$ represents the measured resistance and $R_0$ is the baseline resistance, defined as the average resistance over the initial stable region prior to mechanical loading.

Finger and wrist bending experiments were performed using the same samples over three separate days with repeated bending cycles conducted during individual testing sessions. To improve the repeatability during manual bending and multi-day experiments, the sensor position was kept consistent, the bending displacement was standardized using a ruler as a guide, and the duration of flexed and

relaxed states was timed during each cycle. Representative cycles are presented in the Results section below to compare waveform shape and signal amplitude.

Due to the manual motion of finger and wrist testing, frequency-dependent dynamic loading was further performed using an Aurora Scientific 310C lever arm system (Aurora Scientific Inc., Ontario, Canada) operated in the displacement-controlled mode. These measurements were used to evaluate whether the CNT/BBE–AgNW composites could distinguish controlled cyclic excitation under different defined input frequencies. Testing was performed on the regular sandwich architecture using a sinusoidal displacement-control input with a programmed amplitude of 0.5 channel units. Since this programmed input was not converted to a calibrated physical displacement, results here should be interpreted as a representative dynamic input distinguishability experiment rather than comprehensive study that focuses on fully calibrated frequency-response measurements.

Cyclic loading was applied sequentially at 1, 5, and 10 Hz for 10 s at each frequency, corresponding to 10, 50, and 100 cycles, respectively. A 5-s rest interval was included between frequency steps to allow partial baseline recovery. These frequencies were applied in increasing order here as an initial screening sequence to evaluate the response under progressively faster cyclic inputs. Because the frequency steps were applied consecutively in a fixed order, effects from incomplete viscoelastic recovery, baseline drift, or testing sequence cannot be fully excluded. Future studies should use calibrated physical displacement amplitudes, randomized frequency order, or extended recovery interval trails to systematically quantify frequency-dependent response.

## 3. Results

### *3.1. Morphology and compositional analysis*

The morphology and composition of the CNT/BBE based supporting layer and AgNW interlayer were examined before encapsulation using SEM and EDS. The SEM imaging of the CNT/BBE coated with AgNW demonstrates the composite surface (Figure 3a), appearing continuous and relatively uniform without large-scale aggregation. Furthermore, the SEM imaging reveals the underlying morphology of an interconnected AgNW network (Figure 3b). These interconnected nanowire pathways are important for the multilayer architecture as they are expected to increase conductive junction density across the CNT/BBE composite surface and support interfacial charge transport between elastomer layers.

SEM-EDS elemental mapping was also used to confirm the spatial distribution of the composite and interlayer components. Quantitative EDS analysis further confirmed the presence of Ag in the interlayer region (Figure 3c). The C, O, and Si signals correspond to the CNT/BBE matrix, while the Ag signal confirms the presence of the AgNW layer (Figures 3d–g). Additionally, the Ag distribution was broadly dispersed across the imaged region, supporting the formation of a continuous conductive interlayer as illustrated in Figure 3g.

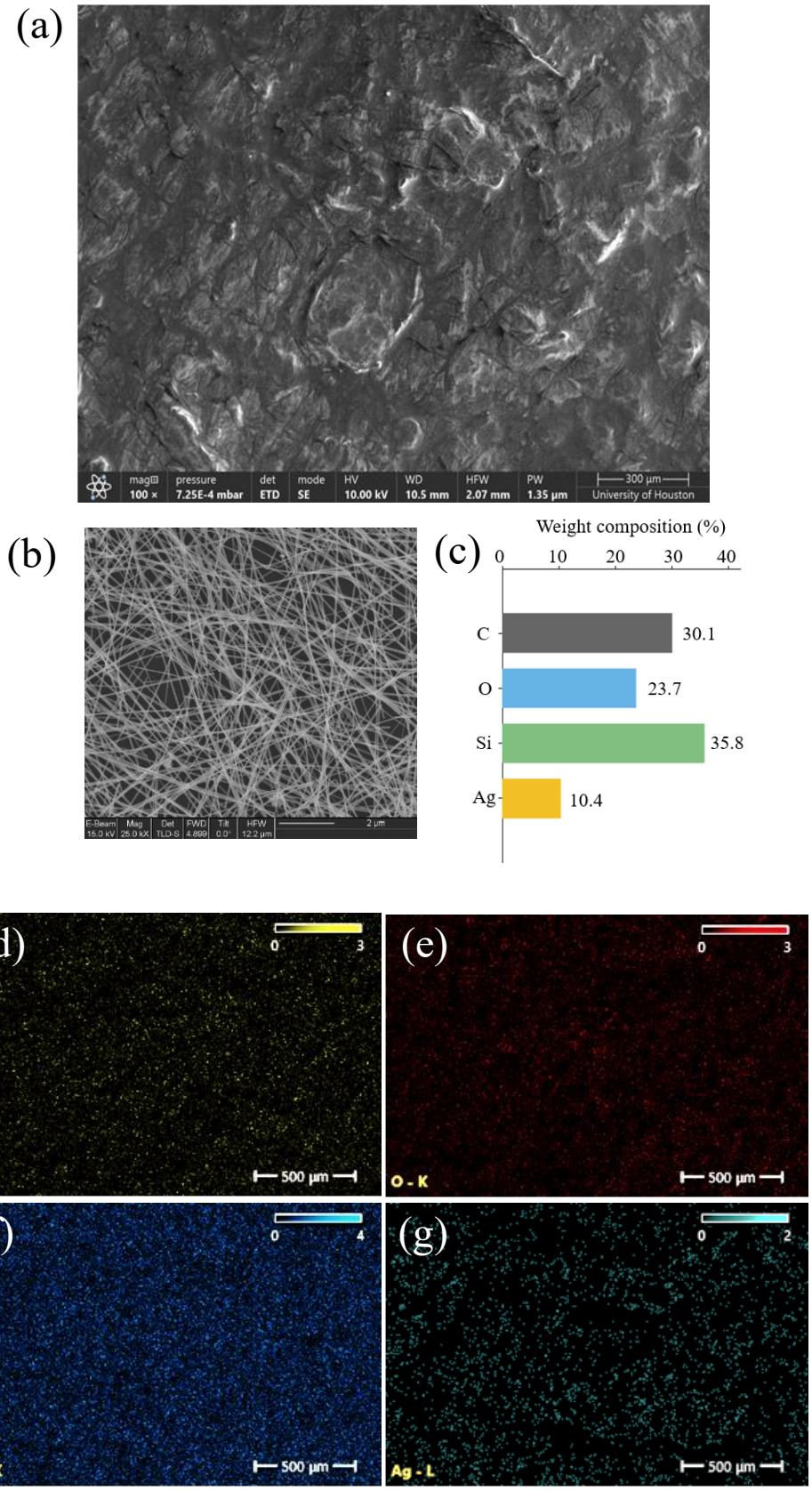



**Figure 3.** Morphology and composition of the AgNW interlayer prior to the top CNT/BBE layer encapsulation. **(a)** SEM image of CNT/BBE after AgNW deposition and **(b)** corresponding high-magnification view of the nanowire network; **(c)** Representative quantitative elemental composition; **(d–g)** EDS elemental maps of C, O, Si, and Ag, respectively.

The SEM and EDS results collectively show that AgNW deposition forms an interconnected conductive network on the CNT/BBE surface. This morphology is central to the sandwich architectural design since the AgNW interlayer functions as an engineered conductive interface that can enhance the through-plane charge transport between CNT/BBE layers.

As compared to the thickness of CNT/BBE layers that were controlled during the casting process by adjusting the volume of precursor solution, the AgNW interlayers were significantly thinner. Therefore, AFM was further used to evaluate the thickness and surface topography of AgNW thin film, and Figure 4 shows one set of characterization results. As can be seen, nanowire layer forms a coating with sub-100 nm of thickness, compared with the millimeter-scale CNT/BBE layers. Given that, variations in total composite thickness are primarily attributed to the CNT/BBE layers in this work, and the coated AgNW interlayers act as thin conductive interfaces within the multilayer architecture of the CNT/BBE-AgNW composites.

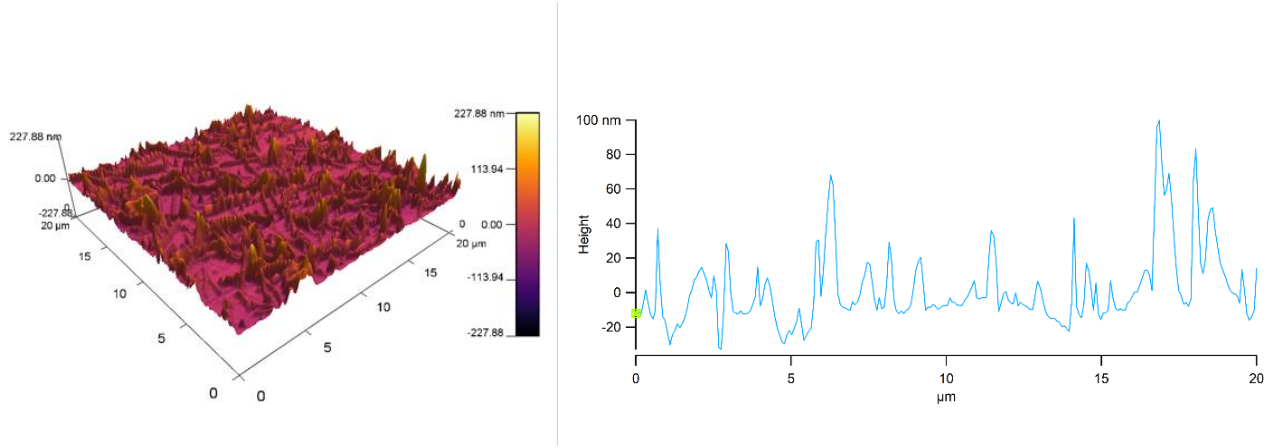



**Figure 4.** AFM characterization of the AgNW interlayer. **(a)** Three-dimensional surface topography and **(b)** corresponding height profile, confirming a nanoscale thickness relative to the CNT/BBE layers.

*3.2. Baseline electrical properties*

The baseline through-plane electrical properties of the CNT/BBE–AgNW sandwich composites were first examined to determine how thickness and interfacial architecture affect charge transport. Figure 5 compares the baseline resistance and calculated conductivity of the regular, thin, and double-sandwich configurations. The corresponding resistance, resistivity, and conductivity measurements are given in Table S1.

As can be seen in Figure 5a, the regular structure, with an overall thickness of approximately 3 mm and one AgNW interlayer, exhibited the highest baseline resistance, with a mean value of ~6.6 KΩ. Reducing the thickness to approximately 2 mm substantially decreased resistance to ~3.04 kΩ. This reduction is consistent with a shorter through-plane transport distance and improved electrical connection between the top and bottom electrodes. The double-sandwich architecture showed the lowest resistance, around 2.02 kΩ, despite having a total thickness of approximately 3 mm. This result indicates that increasing the number of AgNW interlayers can improve through-plane electrical transport even without reducing the overall device thickness.

The calculated conductivity followed the opposite trend in Figure 5b. The regular structure showed the lowest conductivity, while the thin and double-sandwich structures showed enhanced conductivity.

The double-sandwich architecture exhibited the highest conductivity, indicating that the use of additional AgNW interlayer provides more efficient conductive pathways across the multilayer structure. These results suggest that through-plane conductivity of the CNT/BBE-AgNW composites is determined not only by sample thickness but also by the number and placement of conductive interfaces.

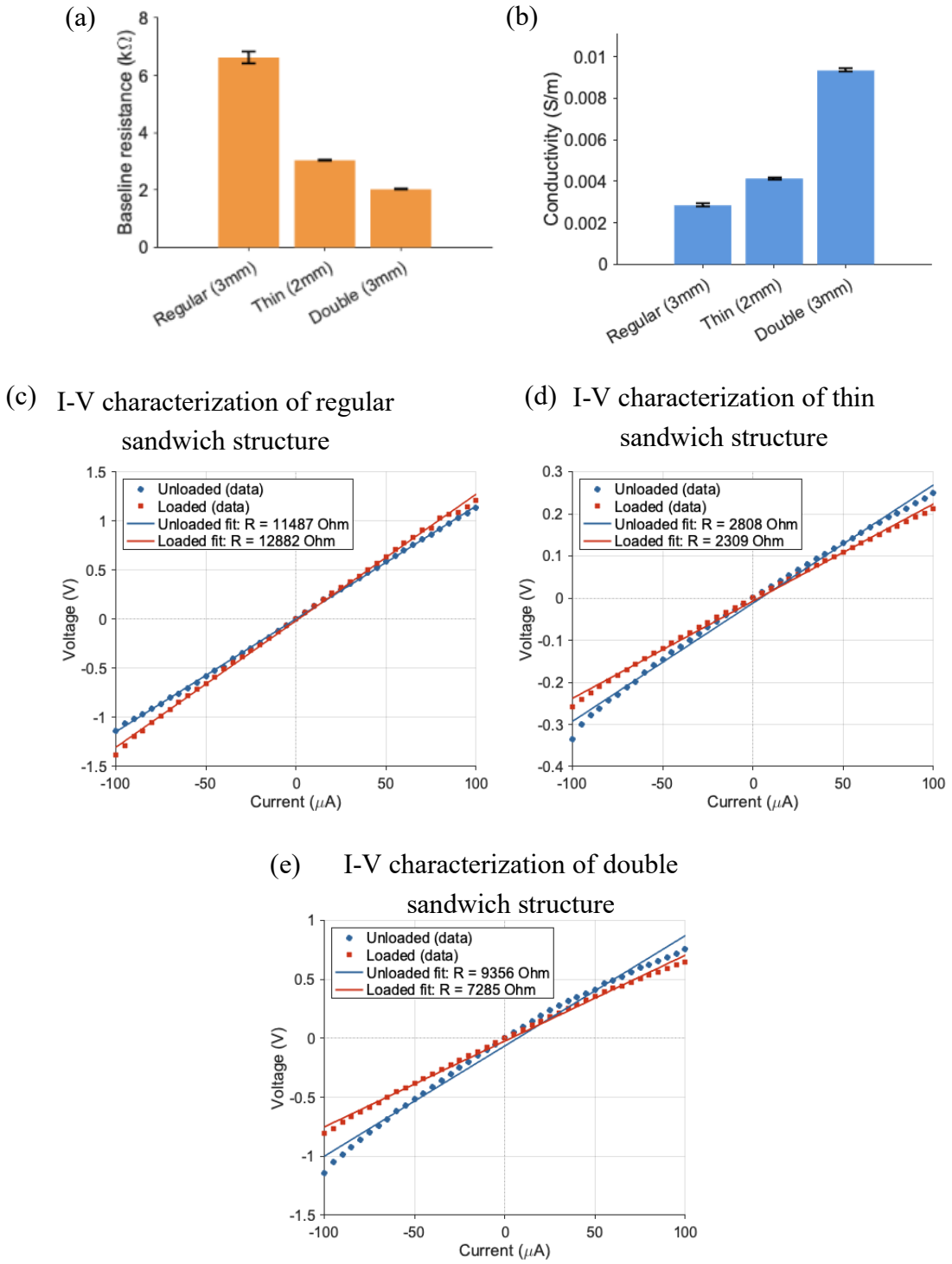



**Figure 5.** Baseline electrical properties of CNT/BBE-AgNW sandwich structures with varying thickness configurations. **(a)** Baseline resistance; **(b)** Calculated conductivity for regular, thin and double sandwich architecture measured under through-plane electrode configuration, and **(c–e)** I-V characterization of the regular, thin, and double sandwich structures, respectively.

Since the through-plane electrode configuration may generate a non-uniform current path, the calculated conductivity values should be interpreted as comparative measures among these architectures rather than absolute intrinsic conductivities. Nevertheless, these trends suggest that reducing transport distance and increasing interfacial conductive density improve baseline electrical transport in multilayer CNT/BBE–AgNW sandwich composites.

To further evaluate the electrical transport characteristics of the multilayer composites and to determine whether the measured resistance was stable over various currents, current-voltage (I-V) characterization was performed on fabricated composites in both unloaded and loaded states. The I-V characterization results are given in Figure 5c–e. During the test, the applied current was swept from −100 μA to +100 μA using a Keithley source-meter, and the resulting voltage was recorded for each architecture. As can be seen, both the unloaded and loaded states for the regular sandwich structure exhibited approximately linear I-V behavior over the tested current range (Figure 5c). Similar approximately linear behavior was observed for the thin and double-sandwich structures, although minor deviations from ideal linearity appeared near the ends of the testing current range in Figure 5d,e.

The approximately linear I-V behavior indicates that the CNT/BBE-AgNW composite showed no strong voltage-dependent resistance within the tested range. The small deviations from ideal linearity may arise from contact effects, interfacial resistance, or non-uniform through-plane current pathways within the multilayer architecture. Therefore, while interfacial and contact-related effects may contribute to charge transport, the resistance and conductivity derived from Equation (1) are appropriate as stable comparative metrics for evaluating architecture-dependent electrical transport.

### *3.3. Wearable bending tests and response analysis*

The electromechanical response of the fabricated CNT/BBE–AgNW composites was evaluated under cyclic finger and wrist bending to illustrate the architecture-dependent behavior under skin-interfaced deformation. The normalized resistance changes, $\Delta R/R_0$, were recorded in real time to compare the regular, thin, and double-sandwich structures as shown in Figure 6. These bending tests were repeated using the same fabricated samples over multiple sessions, and representative cycles are shown to illustrate waveform shape and signal amplitude.

During finger bending, as shown in Figure 6a–c, all three architectures produced repeatable resistance changes in response to deformation. The regular CNT/BBE–AgNW structure exhibited the largest $\Delta R/R_0$ response, indicating high sensitivity to localized bending deformation. This larger resistance modulation is likely associated with greater reconfiguration of conductive pathways within the CNT/BBE–AgNW networks. Because the regular structure contains fewer conductive interfaces than the double-sandwich architecture, deformation-induced disruption or rearrangement of these conductive contacts can produce a larger relative resistance change.

The thin structure showed a lower finger-bending response than the regular structure, while the double-sandwich architectural design showed the smallest response. This trend suggests that improved baseline conductivity may reduce the magnitude of relative resistance modulation. For example, in the double-sandwich structure, the additional AgNW interlayer likely stabilizes conductive transport by providing more parallel conductive pathways. Although this improves conductivity, it also reduces sensitivity to localized deformation because the network is less strongly perturbed by bending.

A different trend was observed during wrist bending in Figure 6d–f. The thin structure produced the largest wrist-bending response, followed by the double-sandwich and regular structures. This behavior may result from improved conformal contact and more efficient strain transfer in the thinner composite. Because wrist bending happens over a broader skin deformation region than finger bending, the reduced thickness of the thin architecture may therefore allow the CNT/BBE–AgNW composite to better follow the curvature of the joint. In contrast, the thicker regular and double-sandwich structures may experience less effective coupling to the wrist surface.

Additionally, the resistance fluctuations during wrist bending were generally smaller than those observed during finger bending. This difference may arise from the larger deformation area and smoother bending geometry of the wrist, which produces more uniform deformation of the CNT/BBE–AgNW composites. Finger bending, by contrast, imposes more localized and geometrically constrained deformation, making the response more sensitive to local contact, sample placement, and conductive network rearrangement.

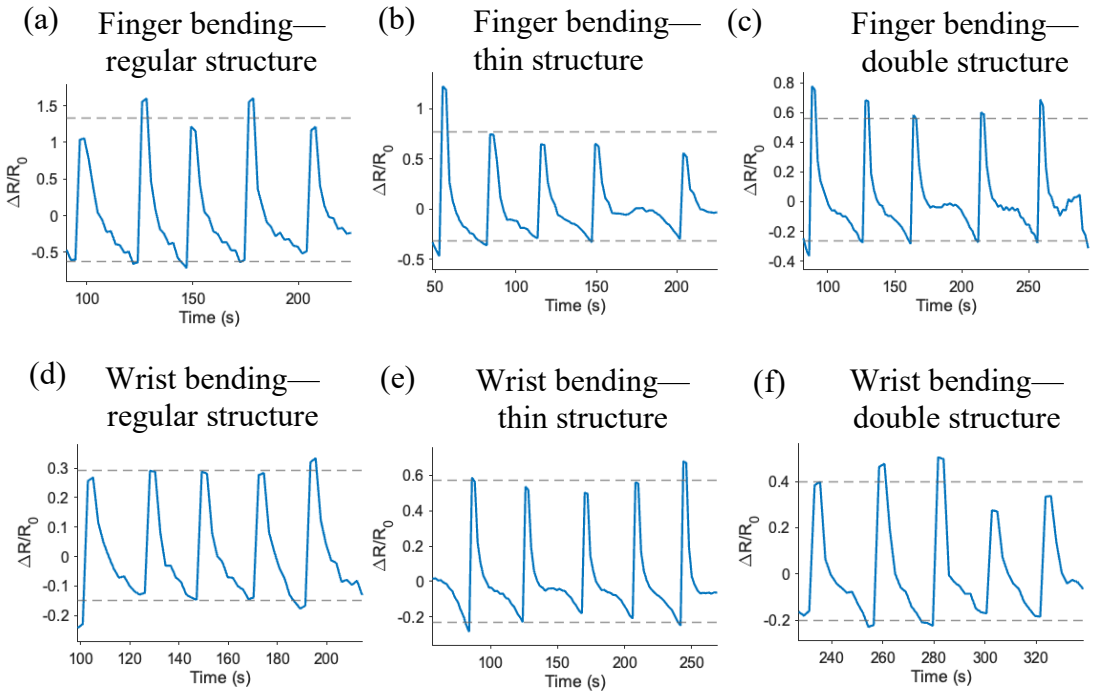



**Figure 6.** Representative electromechanical responses of CNT/BBE-AgNW composites under cyclic bending: normalized resistance ch sanges ($\Delta R/R_0$) during finger bending **(a–c)** and during wrist bending **(d–f)** for regular, thin and double sandwich configurations, respectively.

To further quantify repeated wearable bending behavior, mean response amplitude was calculated from hundreds finger- and wrist-bending cycles, which is shown in Figure 7. The statistical analysis supports the architecture-dependent trends observed in the representative cycles shown in Figure 6: the regular structure showed the largest response during localized finger bending, whereas the thin structure showed the largest response during distributed wrist bending. Because Figure 6 presents representative cycles and Figure 7 summarizes peak amplitudes across repeated tested cycles, the absolute amplitudes are not identical. However, both analyses show consistent architecture-dependent trends. These results support short-term repeatability and response retention of the multilayer composites under the tested

conditions, although extended automated fatigue testing over thousands of continuous cycles remains necessary to fully establish long-term durability.

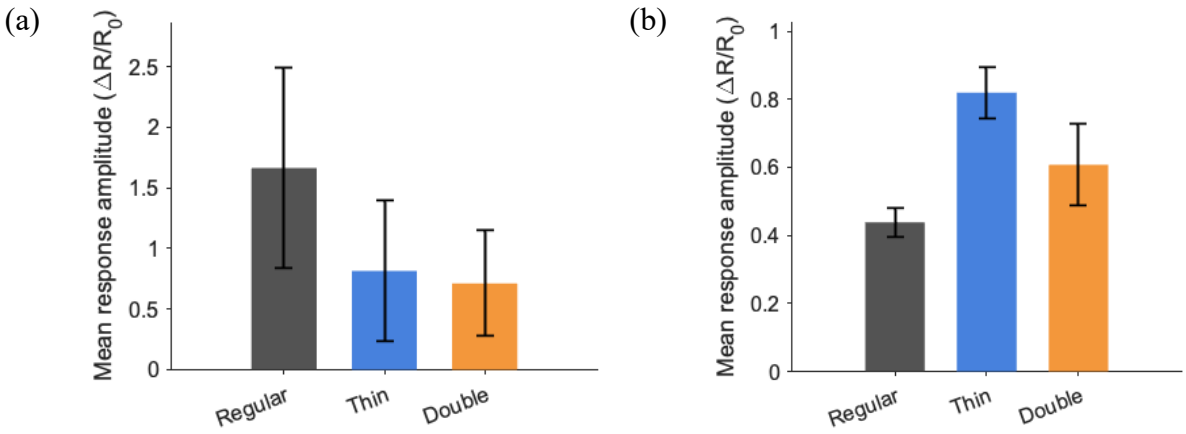



**Figure 7.** Quantitative repeated-bending analysis of the CNT/BBE–AgNW sandwich composites during finger and wrist tests. **(a)** Finger-bending analysis representing localized deformation, and **(b)** wrist-bending analysis representing distributed deformation over a broader joint curvature, where error bars represent cycle-to-cycle variation from repeated bending measurements.

*3.4. Frequency-dependent dynamic sensing response*

While wearable bending tests demonstrated the architecture-dependent responses of CNT/BBE-AgNW composites under skin-interfaced deformation, frequency-dependent loading was conducted to evaluate whether the multilayer composite materials could distinguish controlled cyclic mechanical inputs under defined excitation frequencies. These tests were conducted using the regular sandwich architecture under displacement-controlled loading with an Aurora Scientific lever arm system.

As given in Figure 8a below, the CNT/BBE-AgNW composites exhibited distinguishable resistance responses across the tested frequency range. Because the real-time signal includes baseline drift associated with soft viscoelastic matrix, short 2 s windows were extracted from the middle of each frequency step and detrended using MATLAB to better visualize the dynamic waveform. However, because the tests at 1, 5 and 10 Hz were conducted consecutively in a fixed order, incomplete viscoelastic recovery between steps may contribute to observed baseline drift and apparent frequency-dependent amplitude differences. In addition, the programmed displacement-control input was not converted to calibrated displacement. Thus, these results are interpreted as a qualitative or semi-quantitative demonstration of dynamic input distinguishability rather than a fully calibrated frequency-response analysis. The detrended waveform segments in Figure 8a use the same y-axis scale, allowing direct comparison of the cyclic response at each frequency. The 5 Hz segment shows the clearest periodic waveform, while the 1 and 10 Hz segments show smaller or less regular cycle-to-cycle features. This behavior indicates that the response depends not only on loading frequency, but also on interaction between cyclic deformation, viscoelastic recovery, and conductive-network rearrangement.

The mean resistance change response increased with loading frequency, as given in Figure 8b. This trend suggests that the CNT/BBE–AgNW based composite can distinguish dynamic mechanical inputs across the tested frequency range. However, since signal fluctuation and variation were observed for

individual frequency tested, the frequency-dependent response should be only interpreted as a qualitative or semi-quantitative indicator of dynamic input rather than an exact quantitative measure of waveform amplitude. These limitations are expected for soft viscoelastic conductive composites made of BBEs and highlight the need for future optimization of the multilayer composite for improved stability and signal recovery. Overall, these results support the potential use of CNT/BBE–AgNW architectures for low-to-moderate-frequency dynamic motion detection where relative changes in motion frequency or intensity might be more important than precise waveform reconstruction.

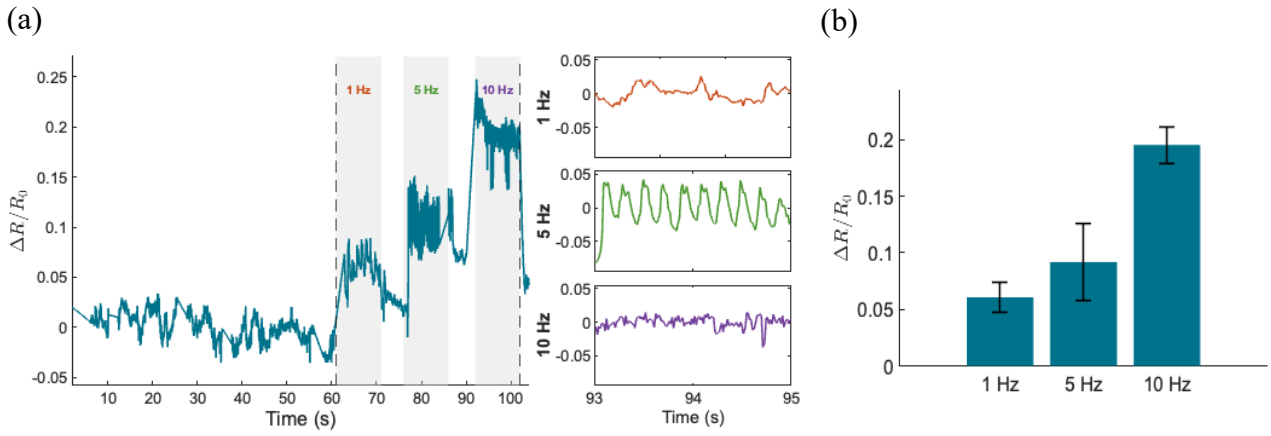



**Figure 8.** Frequency-dependent sensing responses of the CNT/BBE-AgNW composites. **(a)** Dynamic resistance change ($\Delta R/R_0$) of the regular CNT/BBE-AgNW composites under controlled cyclic loading at 1, 5, and 10 Hz, and **(b)** the mean $\Delta R/R_0$ response calculated for each frequency, showing an increasing response with frequency.

*3.5. Post-test interfacial integrity analysis*

To assess whether the multilayer architecture remained mechanically integrated after electromechanical testing, post-test cross-sectional SEM analysis was performed on the regular, thin, and double-sandwich CNT/BBE–AgNW composites. All samples had previously undergone wearable bending and dynamic loading tests described above. As shown in Figure 9, all three architectures exhibited continuous contact between adjacent CNT/BBE layers and AgNW-containing interfacial regions, with no visible interfacial gaps or delamination in cross-sections. These observations provide qualitative evidence that the plasma-assisted, precursor-mediated stacking method produced mechanically integrated multilayer structures that can remain intact under the deformation conditions evaluated in this study. This finding supports the interpretation that the observed architecture-dependent electrical responses arise primarily from differences in conductive pathway modulation, interface density, and mechanical coupling, rather than from gross interfacial failure during testing.

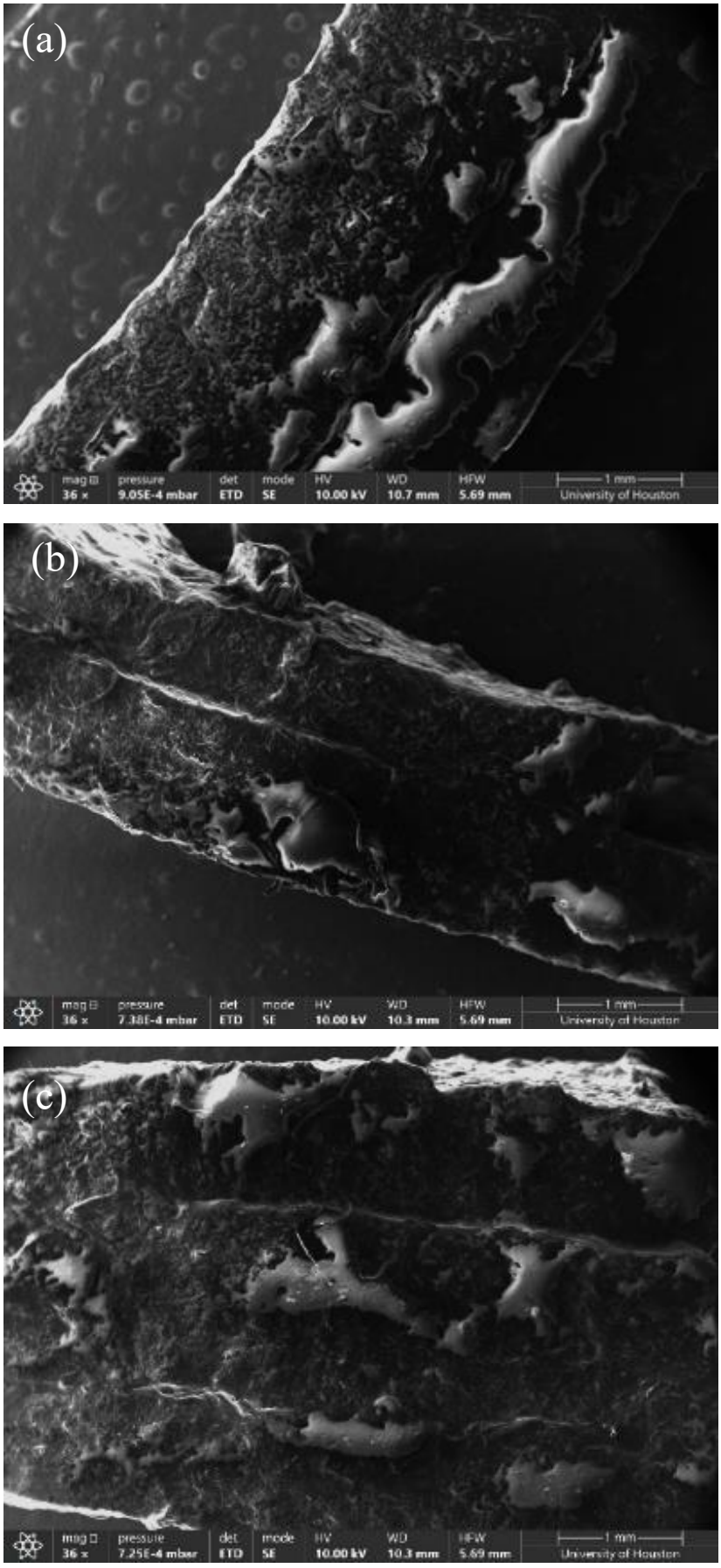



**Figure 9.** Cross-sectional SEM images of **(a)** regular, **(b)** thin, and **(c)** double sandwich architectures, collected post-electromechanical tests, suggesting continuous interfacial contact without delamination.

### *3.6. Discussion*

The results suggest that structural thickness and conductive interface engineering are effective design parameters for regulating the electrical and electromechanical behavior of CNT/BBE–AgNW multilayer composites. Thus, the contribution in this study is the identification of architecture-dependent transport and electromechanical trends in CNT/BBE–AgNW multilayers, rather than the use of CNTs, AgNWs, or conventional piezoresistive sensing principles. The AgNW interlayers function as engineered conductive interfaces within the resulting ultra-soft CNT/BBE-based matrix, while the CNT/BBE layers provide the mechanical compliance and foundational conductive pathways. This combination allows the through-plane transport and deformation-dependent resistance response to be tuned through the multilayer architecture rather than only by changing fillers.

Baseline electrical measurements suggest that both reduced transport distance and increased AgNW interlayer density improve through-plane conductivity. The thin structure lowered resistance by reducing the distance between electrodes, whereas the double-sandwich structure achieved the lowest resistance despite having a thickness comparable to the regular structure. This indicates that adding a second AgNW interface introduces additional conductive junctions and parallel transport pathways, improving electrical continuity across the multilayer composite.

The wearable bending demonstrations show a trade-off between conductivity and deformation-induced resistance modulation. The regular structure produced the largest response during more localized finger bending, likely because its less redundant conductive network undergoes greater rearrangement during deformation. In contrast, the double-sandwich structure exhibited smaller relative modulation, consistent with improved conductive-pathway stability from the additional AgNW interface. The thin structure showed the strongest wrist-bending response, suggesting that reduced thickness improves conformal coupling to broader joint curvature and enhances strain transfer during distributed deformation.

These results also highlight that the preferred architecture may depend on the specific deformation tests. A structure with fewer conductive interfaces may be more responsive to localized deformation, while a thinner structure may be more effective for conformal skin-interfaced motion. A structure with higher interface density may be preferred when lower baseline resistance and transport stability are prioritized. Thus, the CNT/BBE–AgNW multilayer system provides an architecture guided materials framework for tuning the conductivity–response balance in soft electromechanical composites.

The dynamic loading results also suggest that the regular CNT/BBE–AgNW composite can distinguish low-to-moderate-frequency mechanical inputs. However, the observed signal fluctuations indicate that the present materials are better interpreted as qualitative or semi-quantitative dynamic indicators rather than precise waveform-reconstruction devices. These behaviors are consistent with the ultra-soft and viscoelastic nature of the BBE matrix, where polymer relaxation and conductive-network rearrangement occur during repeated deformation.

While this study outlines an architecture-guided design framework for CNT/BBE–AgNW composites, several limitations should be noted. First, the structural variables are not fully independent. Reducing composite thickness changes both the through-plane transport distance and the mechanical compliance of the test sample, while adding an AgNW interlayer may also affect interfacial bonding, internal stress distribution, local deformation, and current pathways. Thus, the observed trends may be interpreted as architecture-level effect rather than isolated single-variable impact. Second, although direct mechanical

testing was not performed for the CNT/BBE-AgNW multilayer architectures, prior literature supports the use of BBE as an ultra-soft matrix platform. To provide additional context, Table S2 lists literature reported mechanical property of related PDMS-based BBEs and conductive BBE composites. Reported Young's modulus values range from approximately 0.63 kPa for pure PDMS-based BBE to about 2.98–10.65 kPa for CNT/BBE hybrid composites [19,26]. These data may support the selection of BBE as a compliant matrix for skin-interfaced applications, but these values are literature benchmarks rather than direct measurements of the CNT/BBE-AgNW multilayer composites. Therefore, the conformability and strain-transfer interpretations should be viewed as architecture-based results supported by electrical response trends and literature reported compliance rather than direct mechanical measurements. Future study should quantify mechanical properties of each architecture to validate differences in compliance, stiffness, stretchability, hysteresis and strain transfer. Third, the conductive-network rearrangement mechanism is inferred from electrical response trends and post-test morphology rather than directly verified during deformation. Future *in situ* imaging or other real-time structural characterization might be used to observe CNT/AgNW junction evolution, interfacial contact changes, and conductive-network rearrangement during deformation. Finally, although the composite maintained cyclic resistance responses from the beginning to the end of hundreds of repeated manual bending sessions, as shown in Figure S1, this work does not include extended automated fatigue testing over thousands of controlled cycles. Therefore, long-term durability, viscoelastic drift, and cycle-induced signal decay remain to be evaluated in future studies using controlled bending angle, frequency, contact pressure, and cycle number.

Overall, this study focuses on the architecture-oriented material design and reveals a clear architecture–property relationship of the CNT/BBE–AgNW sandwich composites. Future optimization and validation are needed before translation into application-ready skin-interfaced devices. For biomedical sensors and wearable applications, investigation in the future may include controlled mechanical testing, loading–unloading hysteresis analysis, extended fatigue tests, and improved signal stabilization. Nevertheless, the present results establish thickness and AgNW interface design as two practical tuning variables for engineering ultra-soft CNT/BBE-based electromechanical materials for skin-interfaced electronics, wearable soft interfaces, and soft robotic systems.

## 4. Conclusion

In this work, multilayer CNT/BBE–AgNW composites with controlled thickness and conductive interfacial architecture were fabricated as ultra-soft electromechanical materials. Comparison of regular, thin, and double-sandwich structures showed that through-plane electrical transport and deformation-dependent resistance response can be tuned by adjusting composite thickness and AgNW interface density. The double-sandwich structure exhibited the lowest baseline resistance, confirming the role of additional AgNW interfaces in enhancing charge transport. Wearable bending demonstrations showed architecture-dependent behavior: the regular structure responded most strongly to localized finger bending, whereas the thin structure exhibited the strongest wrist-bending response because of improved conformal contact. Repeated-bending and frequency-dependent tests also confirmed measurable cyclic responses and low-to-moderate-frequency input distinguishability. In summary, these results establish thickness and interface-density engineering as practical strategies for tuning ultra-soft

CNT/BBE-based conductive composites for future skin-interfaced electromechanical materials, wearable soft interfaces, and soft robotic proprioceptive systems.

## Data availability statement

Data supporting the findings in this study are available within the article and its supplementary material. A supplementary file is provided with this article, which contains baseline through-plane electrical properties of CNT/BBE-AgNW sandwich structures with varying thickness configurations (Table S1), response retention data under repeated manual bending of finger and wrist motions (Figure S1), and the literature reported mechanical properties of related PDMS-based BBE composites (Table S2).

## Declaration of generative AI and AI-assisted technologies

During the preparation of this manuscript, the authors used generative AI (ChatGPT) for image generation to assist in creating the schematic illustration shown in Figure 1a and improve language and readability. The authors reviewed and edited the content and take full responsibility for the content of the manuscript.

## Acknowledgments

This work was funded by the National Science Foundation, grant numbers 2143268 and 2426614.

## Authors' contribution

Investigation, experiments, data collection, data analysis, writing—original draft preparation, A.J.; conceptualization, methodology, investigation, data analysis, supervision, funding acquisition, writing—review and editing, Y.D. All authors have read and agreed to the published version of the manuscript.

## Conflicts of interest

The authors declare no conflicts of interest.

## References

[1] Sony A, Radhakrishnan S, Jelmy EJ, Thomas RM, Kurian T, *et al.* Filler-enhanced conductive elastomers for next-generation electronics applications: a short review. *Discover Appl. Sci.* 2025, 7(11):1330.

[2] Amjadi M, Kyung KU, Park I, Sitti M. Stretchable, skin-mountable, and wearable strain sensors and their potential applications: a review. *Adv. Funct. Mater.* 2016, 26(11):1678–1698.

[3] Rogers J, Someya T, Huang Y. Materials and mechanics for stretchable electronics. *Science* 2010, 327(5973):1603–1607.

[4] Souri H, Banerjee H, Jusufi A, Radacsi N, Stokes A, *et al.* Wearable and stretchable strain sensors: materials, sensing mechanisms, and applications. *Adv. Intell. Syst.* 2020, 2(8):2000039.

[5] Lipomi D, Vosgueritchian M, Tee B, Hellstrom S, Lee J, *et al.* Skin-like pressure and strain sensors based on transparent elastic films of carbon nanotubes. *Nat. Nanotechnol.* 2011, 6(12):788–792.

[6] Yamada T, Hayamizu Y, Yamamoto Y, Yomogida Y, Izadi-Najafabadi A, *et al.* A stretchable carbon nanotube strain sensor for human-motion detection. *Nat. Nanotechnol.* 2011, 6(5):296–301.
[7] Wang X, Jin C, Bai Z. Review of carbon nanotube-based flexible wearable strain sensors: from materials to applications for human body. *Sens. Actuators A Phys.* 2025, 395:117071.
[8] Bauhofer W, Kovacs J. A review and analysis of electrical percolation in carbon nanotube polymer composites. *Compos. Sci. Technol.* 2009, 69(10):1486–1498.
[9] Amjadi M, Pichitpajongkit A, Lee S, Ryu S, Park I. Highly stretchable and sensitive strain sensor based on silver nanowire-elastomer nanocomposite. *ACS Nano* 2014, 8(5):5154–5163
[10] Raman S, Arunagirinathan RS. Silver nanowires in stretchable resistive strain sensors. *Nanomaterials* 2022, 12(11):1932.
[11] Mutiso R, Winey K. Electrical properties of polymer nanocomposites containing rod-like nanofillers. *Prog. Polym. Sci.* 2015, 40:63–84.
[12] Fenta EW, Mebratie BA. Advancements in carbon nanotube-polymer composites: enhancing properties and applications through advanced manufacturing techniques. *Heliyon* 2024, 10(16):36490.
[13] Lin L, Liu S, Zhang Q, Li X, Ji M, *et al.* Towards tunable sensitivity of electrical property to strain for conductive polymer composites based on thermoplastic elastomer. *ACS Appl. Mater. Interfaces* 2013, 5(12):5815–5824.
[14] Kim JH, Hwang JY, Hwang HR, Kim HS, Lee JH, *et al.* Simple and cost-effective method of highly conductive and elastic carbon nanotube/polydimethylsiloxane composite for wearable electronics. *Sci. Rep.* 2018, 8(1):1375.
[15] Wang H, Jiang J, Wang J. The role and progress of silver nanowires in wearable strain sensors for human motion detection. *Alexandria Eng. J.* 2024, 108:706–716.
[16] Pang C, Lee GY, Kim Ti, Kim SM, Kim HN, *et al.* A flexible and highly sensitive strain-gauge sensor using reversible interlocking of nanofibres. *Nat. Mater.* 2012, 11(9):795–801.
[17] Zheng AJ, Chang TFM, Sone M, Chiu WT. Ag Nanowires/polydimethylsiloxane composite thin films for stretchable, transparent electrodes: applications for flexible electronic devices. *ACS Appl. Nano Mate.* 2026, 9(7):3436–3447.
[18] Self J, Reynolds V, Blankenship J, Mee E, Guo J, *et al.* Carbon nanotube composites with bottlebrush elastomers for compliant electrodes. *ACS Polym.* 2021, 2(1):27–34.
[19] Xu P, Wang S, Lin A, Min HK, Zhou Z, *et al.* Conductive and elastic bottlebrush elastomers for ultrasoft electronics. *Nat. Commun.* 2023, 14(1):623.
[20] Kim H, Watkins J, Crosby A. Adhesion and mechanical properties of poly(dimethylsiloxane) bottlebrush elastomers. *Soft Matter* 2023, 19(28):5311–5317.
[21] Xu P, Challa S, Zhang Z, Wu X, Wang S, *et al.* Ultrasoft, elastic, and ionically conductive polyethylene glycol/ionic liquid bottlebrush ionogels. *Mater. Horiz.* 2025, 12(18):7425–7438.
[22] Jackson A, Du Y. Tunable electrical and fatigue performance of carbon nanotube-embedded bottlebrush elastomers via compositional control. *Processes* 2025, 13(11):3613.
[23] Li G, Xue Y, Peng H, Qin W, Zhou B, *et al.* Wide strain range and high sensitivity sandwich structure CNTs/AgNWs/CNTs/TPU strain sensors for human motion detection. *Sens. Actuators A Phys.* 2023, 366:114998.

[24] Li D, Lv X, Guo X, Wei W, Ji J. Flexible strain sensor based on porous polydimethylsiloxane/multiwalled carbon nanotubes and silver nanowire binary composite film for human physiological signals monitoring. *J. Mater. Sci.: Mater. Electron.* 2025, 36(36):2278.

[25] Hu L, Kim HS, Lee JY, Peumans P, Cui Y. Scalable coating and properties of transparent, flexible, silver nanowire electrodes. *ACS Nano* 2010, 4(5):2955–2963..

[26] Hu P, Madsen J, Skov AL. One reaction to make highly stretchable or extremely soft silicone elastomers from easily available materials. *Nat. Commun. 2022,* 13(1):370.